Dewi Jones

Self-archive of publications

Title:	Predictive feed-forward control for a hydroelectric plant
Authors:	Dewi Jones & Sa'ad Mansoor
Published in:	IEEE Transactions on Control Systems Technology, 12(6), 2004, 956-965. DOI: 10.1109/TCST.2004.833405
Version:	This version is the authors' post-print (final draft post-refereeing)
Copyright:	

Predictive feed-forward control for a hydroelectric plant.

Dewi Jones, *Senior Member, IEEE,* and Sa'ad Mansoor

***Abstract*—In this paper it is shown that predictive feed-forward control can be used to help a hydroelectric plant achieve its target for delivered power while operating in Grid (power system) frequency control mode. Due to the fundamental limitation on how fast the water in the supply tunnel can be accelerated by gravity, a hydraulic turbine is always subject to some delay between opening or closing its guide vane and the consequent change in power. Here, it is proposed that the effect of this delay can be alleviated by predicting 3 – 4 seconds ahead what power will be required, based on Grid frequency measurements, and using this as a feed-forward signal to supplement the normal PID feedback controller. Results are presented to show the improved accuracy of power delivery achieved with this approach.**

***Index Terms*— Hydroelectric power; Hydraulic turbine; Feed-forward control; Predictive control; Power system dynamics.**

I. INTRODUCTION

A primary function of the Dinorwig pumped storage hydroelectric station, situated in North Wales, is to regulate the frequency of the electricity supply on the British national grid. Typically, one of its six Units will act in closed loop under PID control, contributing anything between 150MW and 280MW of power to the Grid; this mode of operation is known as Part Load Response (PLR) and will be the focus of this paper. The other Units are used to supply power under manual control and the turbines can go from zero to full power (and vice versa) in 10-15s. The number of Dinorwig Units delivering power at any one time is important here because it changes the total flow of water in the supply tunnel, which affects the operating point of the PLR Unit and hence its dynamic response. The fixed-gain PID governor has been tuned for optimum response under the worst-case condition, when all 6 Units are generating at full power. This situation almost never occurs in practice; indeed it is often the case that only one or two Units are active and the PLR Unit's governor is therefore tuned conservatively.

The National Grid Company maintains the power system frequency within a band of 50Hz ± 0.5Hz at all times. There are usually several frequency regulators, of varying capacity and speed of response, connected to the Grid at any one time. No single station will therefore be called upon to supply all the power necessary to regulate frequency. Instead, stable sharing of the power load between multiple generators is achieved by including in the governors a characteristic that causes generator speed to drop as the load is increased; this is known as the speed regulation or 'droop' characteristic [1]. The goal of Dinorwig in PLR mode is to provide accurate and timely supply of its targeted power contribution, not exclusive control of the frequency to its nominal value. In this paper, we regard this as a problem of tracking a power target that varies with the Grid frequency error. The analysis is based on a known model for the power station and a Grid model identified from power and frequency records, where the latter is used to predict future frequency deviations for a feed-forward controller.

Manuscript received October 17, 2002. The authors are with the School of Informatics, University of Wales, Dean Street, Bangor, Gwynedd LL57 1UT, U.K. (e-mail: dewi@informatics.bangor.ac.uk).

II. SYSTEM MODEL

Dinorwig power station is a complex, nonlinear and time-varying multivariable system. It is modeled in three basic sections - the hydrodynamics, the Turbine/generator and the Control system. Comprehensive dynamic models for simulating hydraulic turbines and their controls have been published by an IEEE Working Group [2] and a specific treatment for Dinorwig is given by Mansoor *et al* [3]. The work here is based on a relatively simple linearised model which is, nevertheless, sufficient to represent the salient dynamics of the response. Fig. 1 is a block diagram of the system.

A. Hydrodynamics

The water supply conduit consists of a long tunnel which divides at a manifold into six separate penstocks for the individual generating Units. The hydrodynamics of the tunnel, penstock and turbine are complex because of the nonlinear relationship which exists between the water velocity, turbine inlet pressure and mechanical power. Under the assumptions of incompressible fluid, rigid conduit and negligible hydraulic friction, Kundur [1] derives a linearised transfer function relating per-unit (p.u.) changes in the mechanical power produced by the turbine (ΔP_m) to per-unit changes in the guide vane position (ΔG) :

$$G_H(s) = \frac{\Delta P_m}{\Delta G} = \frac{-T_w s + 1}{0.5 T_w s + 1} \tag{1}$$

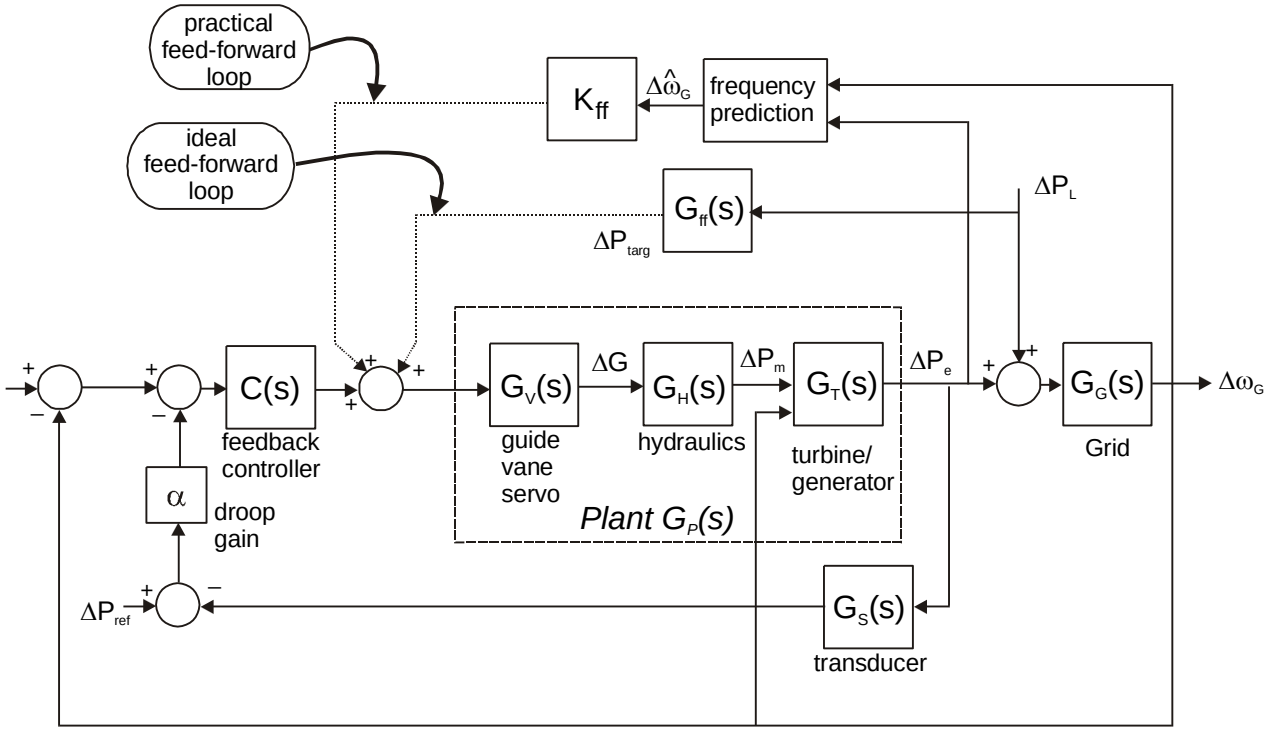

Fig.1 Block diagram of the linearised system model for one turbine/generator operating in PLR mode.

The parameter T_w is known as the 'water starting time' and its value varies with the hydraulic system's operating point. At Dinorwig the value of T_w varies from 0.7s, when one Unit is active, to 2.7s when all 6 Units are operating at full load. Note that transfer function (1) is non-minimum phase. The delay this causes between the control (ΔG) and the output (ΔP_m) is a serious impediment to good tracking performance.

B. Turbine/generator

Based on the well-known 'swing' equation [1], the generated electrical power (ΔP_e) is related to ΔP_m by:

$$\Delta\omega_r = \frac{1}{2Hs}(\Delta P_m - \Delta P_e - K_D\Delta\omega_r) \quad (2)$$

$$\Delta P_e = \frac{K_s\omega_0}{s}(\Delta\omega_r - \Delta\omega_G) \quad (3)$$

where ΔP_e is the per-unit change in electrical power produced by the generator, $\Delta\omega_r$ is the change in angular velocity of the rotor, $\Delta\omega_G$ is the change in angular frequency of the Grid, ω_0 is the rated value of angular velocity, H is the per-unit inertia constant of the turbine/generator, K_D is the per-unit coefficient of damping torque and K_s is the per-unit coefficient of synchronising torque.

C. Guide vane servo

The flow of water through a penstock (and hence the turbine speed and generated power) is controlled by a 2-stage oil hydraulic actuated guide vane. From tests performed on the actuator its transfer function is:

$$G_V(s) = \left(\frac{1}{0.19s+1}\right)\left(\frac{1}{0.4s+1}\right) \quad (4)$$

D. Control System

The control system in Fig. 1 has two feedback loops. The inner loop measures electrical power which is compared with a demand value (which may be set manually by an Operator) to complete a PI feedback loop whose transfer function is:

$$C(s) = \frac{K_p s + K_i}{s} \quad (5)$$

The filter on the transducer is included to reduce measurement noise:

$$G_S(s) = \frac{1}{s+1} \quad (6)$$

The droop gain (α) is imposed on the power error, as explained in section I. The outer loop measures Grid frequency which is compared with the nominal value of 50Hz and the error signal added to the power error. The standard settings for all governors currently in operation at Dinorwig are $K_p = 10$, $K_i = 12$ and $\alpha = 0.01$.

E. Grid

The dynamic model for the Grid is obtained as a 'black box' transfer function in section III. An useful guide to choosing the structure of the identification model is given by the physical model derived by Anderson and Mirheydar [4]. They assume that the Grid response is dominated by two time constants, one associated with the sum of all the inertias of the rotating machines and the other associated with all regulatory mechanisms connected to the Grid. Their transfer function

relates changes in Grid frequency to load imbalance:

$$\Delta\omega_G = K\omega_n^2 T_R\left(\frac{s+1/T_R}{s^2+2\zeta\omega_n s+\omega_n^2}\right)(\Delta P_e - \Delta P_L) \qquad (7)$$

where K is the Grid 'stiffness' (i.e. the steady-state sensitivity of Grid frequency to changes in power), T_R is the time constant of the regulatory mechanisms and ω_n, ζ are the Grid natural frequency and damping factor, respectively. In (7), ΔP_e and ΔP_L affect the Grid frequency in the same manner; essentially the Grid acts as an accumulator whose stored energy is proportional to the synchronous frequency of all the rotating machines connected [1]. The parameters K, T_R, ω_n and ζ are expected to vary with the total 'size' of the Grid load, typically in the range 30 – 50GW in Great Britain. Whilst ΔP_e is known, ΔP_L is the sum of time-varying contributions from many interconnected devices such as motors, heaters, pumps, lamps and power electronic drives. Equation (7) indicates that it is appropriate to regard ΔP_L as an additive disturbance whose characteristics can be identified from recorded data.

III. Identification of the Grid System

A. Non-parametric system identification

The power output of each Unit at Dinorwig and the Grid frequency are routinely sampled at 1s intervals and archived. A typical daily record (86400 points) is shown in Fig. 2, where the total station power is the sum of the contributions by individual Units. The normalisation to the per-unit scale is given by:

$$Power(p.u.) = \frac{Power(MW)}{30GW} \quad \text{and}$$

$$frequency(p.u.) = \frac{frequency(Hz) - 50}{50} \qquad (8)$$

The intervals of negative power occur when water is being pumped back to the upper lake, usually at night. Sharp changes in the power flow at Dinorwig occur as Units are brought on- or off-line. The frequency is a random variable which remains mostly within a band of about ±0.1Hz of the nominal.

Insight into the dynamics of the process which produced the record in Fig. 2 can be obtained by nonparametric identification methods [5]. These are implemented in the Matlab Systems Identification Toolbox [6]. In the time domain, the step response from the input ΔP_e to the output $\Delta\omega_G$ can be estimated by fitting a high-order, non-causal FIR model to the data. Computation of the step response for several daily records during the year 2001 showed a high degree of consistency – the result for March 4th is shown in Fig. 3. The step response is underdamped ($\zeta \approx 0.57$) and has a natural frequency $\omega_n \approx 0.35$r/s. Fig. 3 also exhibits a significant response for negative delay which is an indicator of feedback from the output to the input.

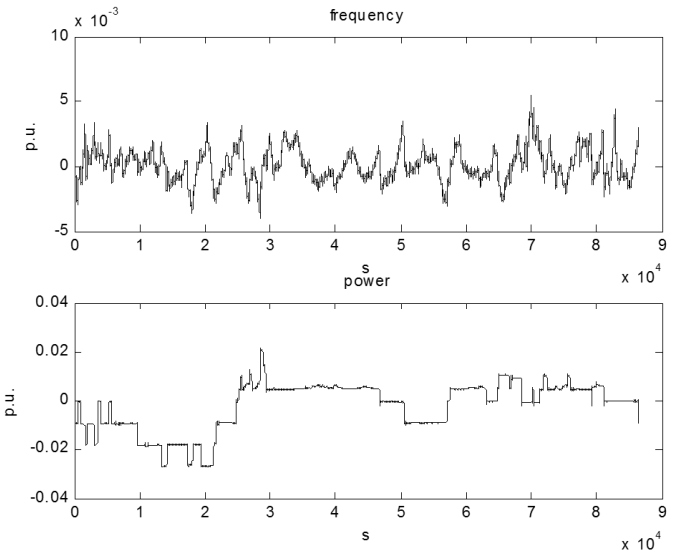

Fig. 2 Record of per-unit Grid frequency and total power flowing at Dinorwig for the 24-hour period of 4th March 2001.

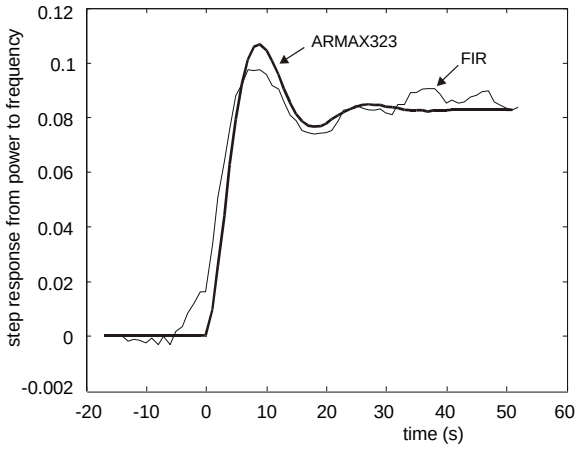

Fig. 3 Estimated step responses for the data record of Fig. 2.

Two forms of feedback are known to exist:

- Low-frequency feedback as the National Grid Company manually directs Units to come on- or off-line to counteract trends of the frequency away from its nominal 50Hz;
- High-frequency feedback when Dinorwig operates one or more of its Units in PLR mode.

The power spectral density function of the Grid frequency record is shown in Fig. 4. It reveals that, except for the small peak which appears in the range 0.3 – 0.4 r/s (which is consistent with the step response), it has a 20dB/decade roll-off with frequency. Together, Figs. 3 and 4 infer that the basic Grid model consists of (a) a low-order dynamic relationship between $\Delta\omega_G$ and ΔP_e which is consistent with (7), and (b) an additive 'random walk' term to represent the effect on $\Delta\omega_G$ of the unknown variation in ΔP_L.

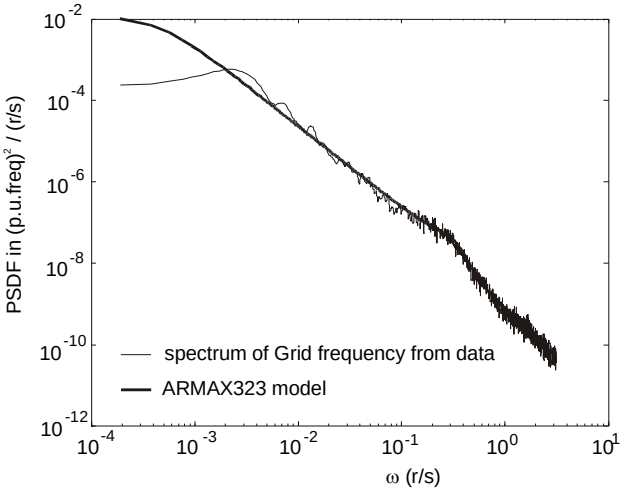

Fig. 4 Power spectral density function of the Grid frequency record of Fig. 2 and the model identified from the data.

B. Parametric system identification method

A parametric model can be found by applying the powerful prediction-error methods described by Ljung [5]. Transfer function (7) indicates that both the input ΔP_e and disturbance ΔP_L are affected by the Grid dynamics, which is characteristic of the equation-error family of model structures. Describing ΔP_L as a moving average of white noise leads to the discrete time ARMAX model (9):

$$\begin{aligned}\Delta\omega_G(k) + a_1\Delta\omega_G(k-1) + ... + a_{n_a}\Delta\omega_G(k-n_a) = \\ b_1\Delta P_e(k-1) + b_2\Delta P_e(k-2) + ... + b_{n_b}\Delta P_e(k-n_b) + \\ w(k) + c_1 w(k-1) + c_1 w(k-1) + ... + c_{n_c} w(k-n_c)\end{aligned} \quad (9)$$

where w(k) is a zero mean Gaussian white noise sequence. Let

$$\begin{aligned}A(q) &= 1 + a_1 q^{-1} + ...a_{n_a} q^{-n_a} \\ B(q) &= \quad b_1 q^{-1} + ...b_{n_b} q^{-n_b} \\ C(q) &= 1 + c_1 q^{-1} + ...a_{n_c} q^{-n_c}\end{aligned} \quad (10)$$

where q is the forward shift operator. Then:

$$A(q)\Delta\omega_G(k) = B(q)\Delta P_e(k) + C(q)w(k) \quad (11)$$

and : $$\underline{\theta} = [a_1.....a_{n_a} \quad b_1.....b_{n_b} \quad c_1.....c_{n_c}] \quad (12)$$

where $\underline{\theta}$ is the vector of parameters to be determined. A one-step-ahead predictor for the frequency deviation is [5]:

$$C(q)\Delta\hat{\omega}_G(k\,|\,\underline{\theta}) = B(q)\Delta P_e(k) + [C(q) - A(q)]\Delta\omega_G(k) \quad (13)$$

where $\Delta\hat{\omega}_G(k\,|\,\underline{\theta})$ is the conditional expectation of the frequency deviation at time k given information up to time (k-1). The prediction error is given by :

$$\varepsilon(k,\underline{\theta}) = \Delta\omega_G(k) - \Delta\hat{\omega}_G(k\,|\,\underline{\theta}) \quad (14)$$

and the identification method used here [6] finds the value of $\underline{\theta}$ which minimises the quadratic criterion:

$$V_N(\underline{\theta}, Z^N) = \frac{1}{N}\sum_{k=1}^{N}\frac{1}{2}\varepsilon^2(k,\underline{\theta}) \quad (15)$$

where Z^N is the batch data [$\Delta\omega_G(1)$, $\Delta P_e(1)$, $\Delta\omega_G(2)$, ΔPe(2) ……. $\Delta\omega_G(N)$, $\Delta P_e(N)$]. The minimisation is done by iterative numerical search.

C. Results for parametric identification.

Experimentation with this method applied to several daily records showed that the lowest-order function which gives a good approximation to the step response and spectrum of Figs. 3 and 4 is the ARMAX323 model. For the record of Fig. 2 the model is :

$$\begin{aligned}\Delta\omega_G(k) = &-2.643\Delta\omega_G(k-1) + 2.403\Delta\omega_G(k-2) \\ &- 0.759\Delta\omega_G(k-3) + 0.00959\Delta P_e(k-1) \\ &- 0.00958\Delta P_e(k-2) - 1.131w(k-1) \\ &+ 0.16w(k-2) + 0.192w(k-3)\end{aligned} \quad (16)$$

The continuous-time ZOH-equivalent transfer function for (16) is calculated using the method described by Franklin, Powell and Workman [7] and implemented in the Matlab Control System Toolbox [8]:

$$\begin{aligned}\Delta\omega_G = &\frac{0.005351s^2 + 0.0111s + 3.432\times10^{-6}}{s^3 + 0.2757s^2 + 0.1337s + 5.896\times10^{-5}}\Delta P_e \\ &+ \frac{s^3 + 1.658s^2 + 0.7773s + 0.2552}{s^3 + 0.2757s^2 + 0.1337s + 5.896\times10^{-5}}w\end{aligned} \quad (17)$$

The first part of this transfer function has one zero and one pole which are nearly co-located and can be reduced to (18), which is directly comparable with Anderson & Mirheydar's model (7):

$$\frac{\Delta\omega_G}{\Delta P_e} = \frac{0.005376\ s + 0.01107}{s^2 + 0.2747\ s + 0.1334} \quad (18)$$

Comparing coefficients gives $\omega_n \approx 0.36$r/s, $\zeta \approx 0.38$, $T_R \approx 0.49$s and K = 0.083 as the parameter values for (7). De-normalising:

$$\frac{\Delta P_e(p.u.)}{\Delta\omega_G(p.u.)} = \frac{1}{K} = \frac{\Delta P_e / 30GW}{\Delta\omega_G / 50Hz} \qquad \therefore \frac{\Delta P_e}{\Delta\omega_G} = \frac{723MW}{0.1Hz}$$

gives the Grid 'stiffness', i.e. generating an extra 723MW causes a 0.1Hz change in frequency, after all the regulators on the Grid have settled. The accuracy with which the value of the steady-state parameter K can be identified is rather poor, because it is derived via the 'system' model. This requires

recognising those changes in $\Delta\omega_G$ caused solely by changes in the (known) input power ΔP_e, which consists only of infrequent and rather small 'steps'. In contrast, the transient parameters ω_n and ζ are derived via the 'noise' model and are relatively accurate, because the system is persistently excited by the random disturbance ΔP_L. It is concluded that the transfer function (17) is a satisfactory low-order 'average' dynamic model for the Grid.

IV. CONTROL SYSTEM

A. Feedback analysis

The effect of varying T_W on the power feedback loop is considered here, where the Grid is (temporarily) regarded as an infinite busbar so that $\Delta\omega_G \equiv 0$. From (2) and (3), the turbine/generator transfer function is then:

$$G_T(s) = \frac{K_s\omega_0 / 2H}{s^2 + \frac{K_D}{2H}s + \frac{K_s\omega_0}{2H}} \qquad (19)$$

Ignoring (for now) the feed-forward paths in Fig. 1, the open loop transfer function between the measured and reference powers is:

$$\frac{\Delta P_{meas}}{\Delta P_{ref}} = \alpha C G_V G_H G_T G_S \qquad (20)$$

For the standard tuning parameters $K_p = 10$, $K_i = 12$, $\alpha = 0.01$ and $T_W = 2.7$s (the case for 6 Units in operation), the corresponding step response in Fig. 5a (full line) indicates a well-tuned, slightly underdamped response. Note the significant initial delay of 2 – 3s before the generated power begins to increase.

When the value of T_W is changed to 0.7s, corresponding to the case of one Unit in operation, the step response is given by the thin line in Fig. 5a and is seen to be over-damped, i.e. the loop is tuned conservatively. An attempt to rectify this by increasing the loop gain by a factor of 2.4 yields the step response of Fig. 5b (thin line), which is fast and well-damped. However, the response during 6 Unit operation now becomes very underdamped and quite unacceptable (Fig 5b thick line). It is concluded that simply increasing the PI gains will not give satisfactory performance.

B. The power target and ideal feed-forward

As stated in the Introduction, the goal in PLR mode is to match the generated power to a 'power target' that varies with the Grid frequency error according to (21):

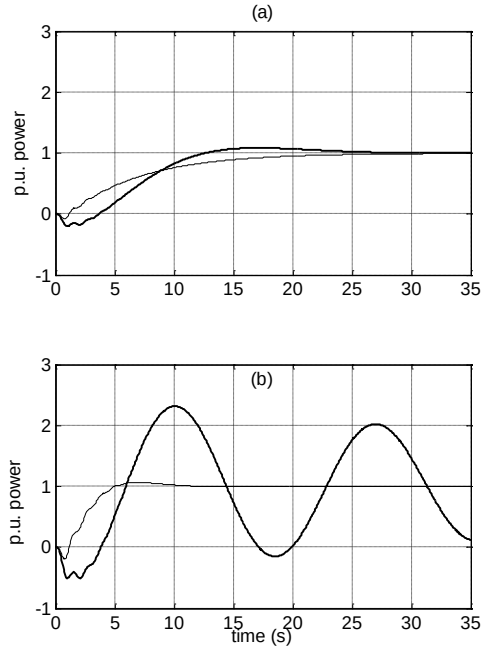

Fig. 5 Comparison of closed loop power generated in response to an unit step increase in Grid load for (a) $K_p = 10$, $K_i = 12$, $K_d = 2$ (b) $K_p = 24$, $K_i = 28.8$, $K_d = 2$ where the thick lines denote $T_W = 2.7$s (6 Unit operation) and the thin lines denote $T_W = 0.7$s (1 Unit operation).

$$\Delta P_{t\,\mathrm{arg}} = (\omega_{sp} - \omega_G)\frac{P_{rated}}{\alpha\omega_{sp}} \qquad (21)$$

For $\omega_{sp} = 50$Hz, $P_{rated} = 300$MW and $\Delta\omega_G = (\omega_G - \omega_{sp})$:

$$\frac{\Delta P_{t\,\mathrm{arg}}}{\Delta\omega_G} = -\frac{6}{\alpha}\frac{MW}{Hz}$$

and normalising to 300MW and 50Hz, the per-unit power target is:

$$\Delta P_{t\,\mathrm{arg}}(p.u.) = -\frac{6}{\alpha}\frac{1/300}{1/50}\Delta\omega_G(p.u.) = -\frac{\Delta\omega_G}{\alpha}(p.u.) \qquad (22)$$

Suppose that in the model of Fig. 1, a step increase in load imbalance ΔP_L is imposed on the Grid at t = 3s, causing the frequency to drop, as shown in Fig. 6(c). The corresponding power target is shown in Fig. 6(a) and it is evident that the generated electrical power tracks it poorly under feedback control alone. In particular, there is a substantial delay between the power target and the generated power. The realisation in (22) that the power target is proportional to the frequency error is important because it means that, if the future frequency error is known, then a feed-forward signal for the power loop can be produced to improve the reference tracking.

Suppose now that the 'ideal' feed-forward loop in Fig.1 is connected so that the load disturbance ΔP_L is filtered by the transfer function, G_{ff}, and added to the output of the feedback controller. This presents a fundamental difficulty because ΔP_L

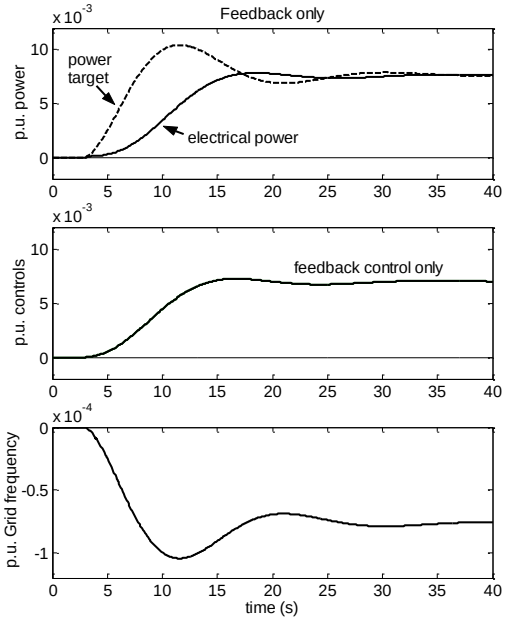

Fig. 6 Response to a step increase in Grid load at t = 3s with feedback control only, (a) generated and target power, (b) controls, (c) Grid frequency.

cannot be measured. The analysis therefore proceeds in a manner similar to that discussed by Goodwin, Graebe & Salgado [9], although the inner power loop makes it a little different from the standard case. In Fig. 1, let the plant transfer function be $G_P = G_v G_H G_T$. Then:

$$\begin{aligned} \Delta\omega_G &= G_G(\Delta P_L + \Delta P_e) \\ \Delta P_e &= G_P G_{ff}\Delta P_L - \alpha C G_P \Delta P_e - C G_P \Delta\omega_G \end{aligned} \tag{23}$$

Eliminating ΔP_L :

$$\Delta P_e = \frac{(G_P G_{ff} - G_P G_G C)}{(G_G + \alpha G_P G_G C + G_P G_G G_{ff})}\Delta\omega_G \tag{24}$$

The required feed-forward signal is ΔP_{targ} so, by substituting from (22) :

$$\frac{\Delta P_e}{\Delta P_{t\,\mathrm{arg}}} = -\alpha\frac{(G_P G_{ff} - G_P G_G C)}{(G_G + \alpha G_P G_G C + G_P G_G G_{ff})} = 1 \tag{25}$$

for ideal tracking. Hence

$$G_{ff} = \frac{-G_G/\alpha}{G_P(1+G_G/\alpha)} \tag{26}$$

The magnitude of the changes in the load imbalance power are much greater than those generated locally during operation in PLR mode, i.e. $|\Delta P_L| >> |\Delta P_e|$ so that $G_P \cong \Delta\omega_G / \Delta P_L$ allowing (26) to be approximated as:

$$G_{ff} = \frac{-1/\alpha}{G_P}\frac{\Delta\omega_G}{\Delta P_L + \alpha\Delta\omega_G} \tag{27}$$

Noting again that $|\alpha\Delta\omega_G| \approx |\Delta P_e| << |\Delta P_L|$, (27) reduces to:

$$G_{ff} = \frac{-1/\alpha}{G_P}\frac{\Delta\omega_G}{\Delta P_L} = \frac{\Delta P_{t\,\mathrm{arg}}}{\Delta P_L} \tag{28}$$

and:

$$\Delta P_{t\,\mathrm{arg}} \cong \frac{-1/\alpha}{G_P}\Delta\omega_G \tag{29}$$

Equation (29) indicates that the feed-forward signal is formed by filtering the measured frequency through the inverse of G_P which, consisting of the hydrodynamics and gate vane hydraulics blocks, is essentially a delay. Thus a prescient feed-forward controller would be required as its inverse.

The effectiveness of such a non-causal controller is demonstrated in Fig. 7 where the load step is applied to the Grid model at t = 3s but to the feed-forward controller at t = 0. The feed-forward component in Fig. 7(b) anticipates the disturbance and the feedback control is relegated to a corrective role, taking account of any differences between the real plant and its assumed model. By appropriate adjustment of the prediction time and the feed-forward gain, excellent tracking of the power target is achieved.

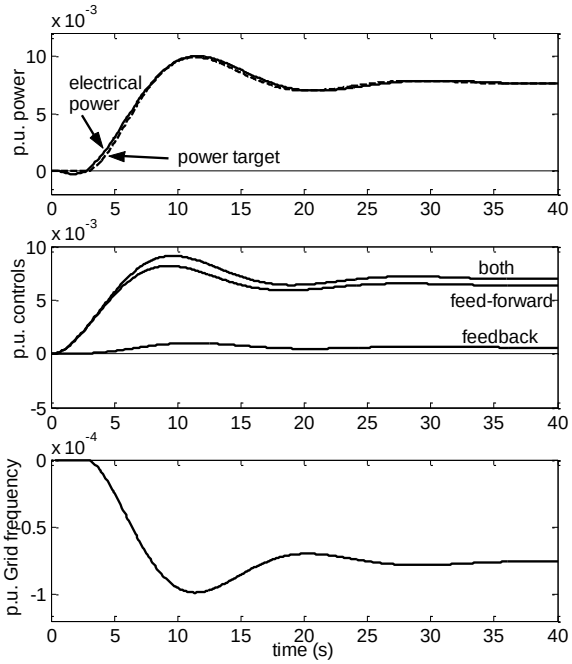

Fig. 7 Response to a step increase in Grid load with both feedback and feed-forward control, (a) generated and target power, (b) controls, (c) Grid frequency.

Clearly, this hypothetical controller is impossible to achieve so the prescience of the feed-forward controller must be approximated by a prediction of the frequency error. This approximate, but feasible, controller will not be as effective as the ideal but substantial gains may nevertheless be obtained.

C. Frequency prediction

For the ARMAX323 model, the 1-step-ahead predictor (13)

is given by:

$$\begin{aligned}\Delta\hat{\omega}_G(k) = &-2.643\Delta\omega_G(k-1) + 2.403\Delta\omega_G(k-2)\\ &- 0.759\Delta\omega_G(k-3) + 0.00959\Delta P_e(k-1)\\ &- 0.00958\Delta P_e(k-2) - 1.131[\Delta\omega_G(k-1)\\ &- \Delta\hat{\omega}_G(k-1)]\\ &+ 0.16[\Delta\omega_G(k-2) - \Delta\hat{\omega}_G(k-2)]\\ &+ 0.192[\Delta\omega_G(k-3) - \Delta\hat{\omega}_G(k-3)]\end{aligned} \quad (30)$$

Equation (30) is straightforward to iterate forward in time to obtain 2-step-ahead predictors etc. Applying (30) to the data of Fig. 2 (and noting that this is the record from which the ARMAX323 model was derived), the estimates $\Delta\hat{\omega}_G$ can be compared with the actual values $\Delta\omega_G$. The upper set of curves in Fig. 8 shows an extract of the predictions for the 1 and 2-step-ahead cases, where the predictions are plotted at the time they are made. Generally, the 1-step-ahead predictions are good but the accuracy deteriorates as the number of steps ahead increases. The quality of the predictions can be quantified by using the 'goodness-of-fit' criterion [5] for a j-step-ahead predictor:

$$R^2 = \left\{1 - \frac{\sum_1^N \left|y(k) - \hat{y}_j(k)\right|^2}{\sum_1^N \left|y(k) - \bar{y}\right|^2}\right\} \quad (31)$$

where $\bar{y}$ is the mean value of y(k).

A value of R^2 = 100% in (31) indicates a perfect fit while a value of R^2 = 0% signifies a fit that is no better than predicting $\hat{y}(k) = \bar{y}$. The top half of Table I shows how R^2 varies with j, based on 2000 points of the data record and indicates an excellent 'fit' for all values of j.

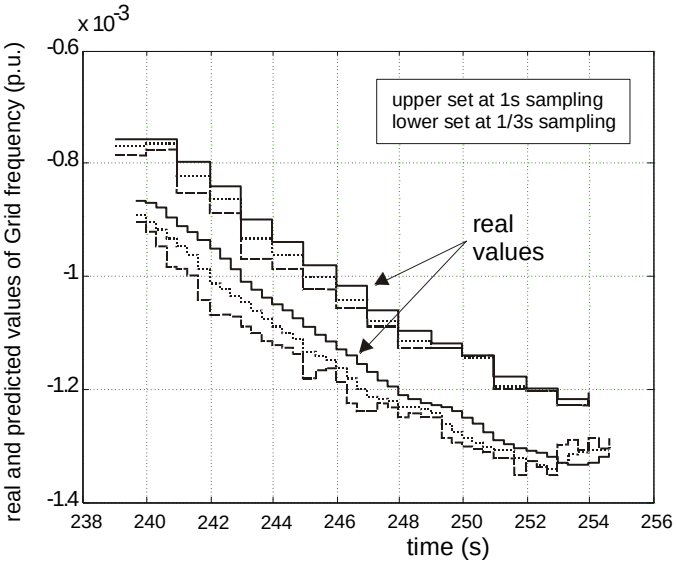

Fig. 8 Comparison of j-step-ahead predictions for 1s and 1/3s sampling rates.

Equation (31) normalises to the mean $\bar{y}$ and emphasises the long-term correspondence between the actual and predicted values which, in this case, is very good. This occurs because the relatively short sampling period of 1s allows long term variation of the Grid frequency to be followed accurately. It is, however, misleading as a measure of the short-term prediction which is of interest here. A better quality indicator is obtained by normalising to the 'trivial' predictor $\hat{y}(k) = y(k-1)$, giving

$$J^2 = \left\{1 - \frac{\sum_1^N \left|y(k) - \hat{y}_j(k)\right|^2}{\sum_1^N \left|y(k) - y(k-1)\right|^2}\right\} \quad (32)$$

Table I shows that J^2 has much lower values than R^2 and suggests that predictions using (30) are an useful - but hardly exceptional - improvement on simply using the previous measurement.

TABLE I
COMPARISON OF PREDICTIVE ABILITY FOR J-STEP-AHEAD PREDICTORS

	time ahead (s)	r.m.s. prediction error $\times 10^{-4}$	R^2 (%)	J^2 (%)
1s samples	1	0.238	97.8	18.1
	2	0.429	96.1	16.0
	3	0.592	94.6	15.6
1/3s samples	1/3	0.0025	99.9	97.6
	1	0.1	99.1	50.1
	2	0.214	98.0	26.1
	3	0.213	98.0	42.4

More emphasis would be given to the high-frequency behaviour of the system by sampling at a higher rate but the 1s data was the only record easily available. The data of Fig. 2 was therefore re-sampled at a 1/3s interval by interpolation with pre-filtering. An ARMAX969 model was obtained for the complete, re-sampled record of March 4th - this order was chosen simply to match its maximum delays to the ARMAX323 model. The improvement in predictive quality is evident in both Fig. 8 (bottom traces) and the bottom half of Table 1.

Note that the offset between the values for the 1s and 1/3s cases in Fig. 8 is due to the de-trended values being displayed for the latter, for clarity of the diagram. The J^2 values for the 1/3s sampling period are significantly better than for 1s and give a substantial improvement on the trivial predictor. Again the prediction quality deteriorates with length of look-ahead. Fig. 8 shows that the 2s-ahead predictions are more noisy and also 'under-predict' by about 1/3s. This becomes a second or more in the case of the 3s-ahead predictor. This is likely to affect the feed-forward controller adversely when operating with a high value of T_W. A significant advantage of the shorter sampling period is that smoother control is possible - the extra on-line computation is not a significant trade-off factor. It is concluded that the ARMAX969 model is capable of predicting what the Grid frequency will be, a short time in the future, and

can be used as a feed-forward signal.

D. Predictive feed-forward

The ARMAX969 predictor was included in the simulation (marked 'practical' feed-forward loop in Fig.1) with T_W = 1s. The Grid model was represented by its corresponding continuous-time version. The simulation was first run with zero feed-forward gain, K_{ff} = 0. Fig. 9 is an extract from the power record which shows that the electrical power tracks its target poorly, especially when it is changing rapidly. When the 2s-step-ahead predictor is included, with K_{ff} = 65, the tracking is much better as shown in Fig. 10, although the electrical power now exhibits more short-term variation. The frequency prediction used to provide the feed-forward signal is given in Fig. 11. A quantitative assessment of the effect of feed-forward is obtained by computing the R.M.S. value of the error between the delivered power and the target. Fig. 12 shows the power error to be 2.7MW rms when feedback alone is used, which reduces to 0.88MW rms when feed-forward is introduced, a 67% improvement in tracking error.

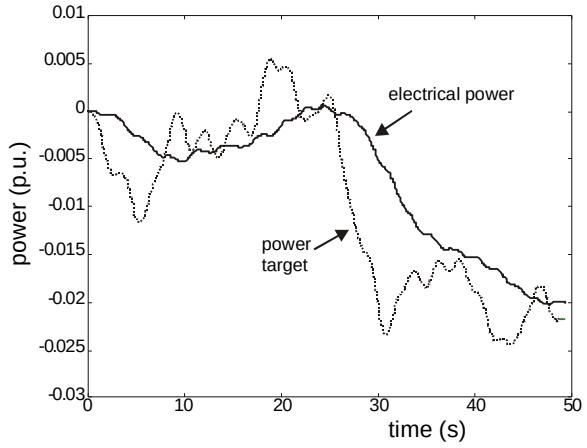

Fig. 9 Tracking of electrical power to its target, FF gain = 0.

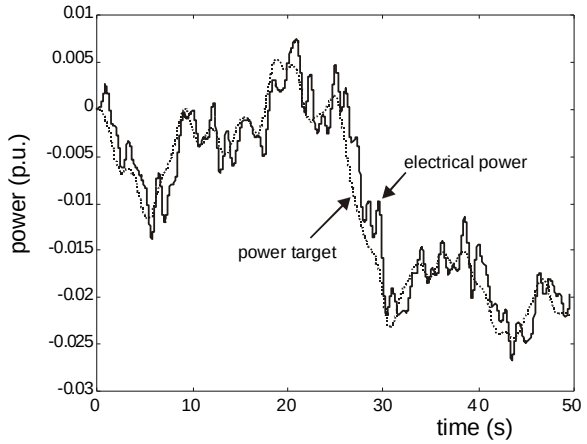

Fig. 10 Tracking of electrical power to its target, FF gain = 65 and 2s-ahead prediction.

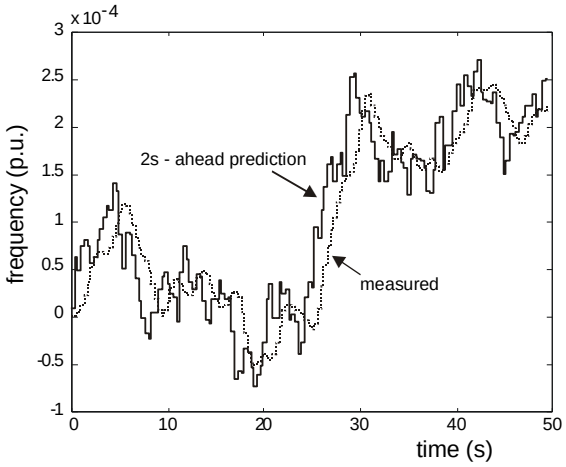

Fig. 11 Comparison of 2s-ahead predicted frequency with measured frequency.

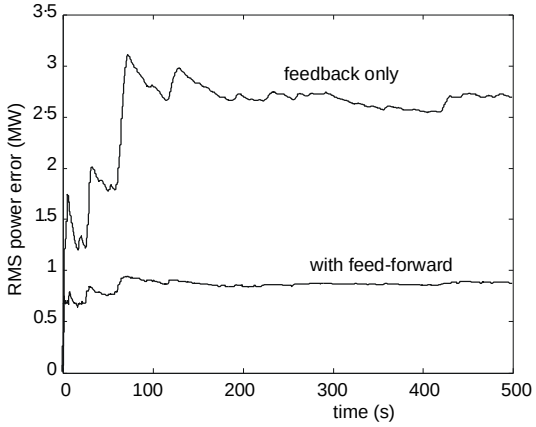

Fig. 12 RMS value of the error between the power delivered and the power target.

V. OPTIMISATION AND SENSITIVITY ANALYSIS.

The results in section IV show that the feed-forward strategy can yield substantial improvements when correctly tuned. In this section, the effect on the rms power error of choosing different values of the main predictor parameters, i.e. gain K_{ff} and prediction time T_p, is investigated. Further, it is of interest to investigate how the rms power error is affected by a mismatch between the real process and the assumed model. The sensitivity is considered for 2 cases: (a) when T_W is changed from 0.7s to 2.7s while T_p is kept constant at 2s and (b) when the model used in the predictor differs from the actual Grid characteristics.

A. Optimisation of gain and prediction time

Here, both the Grid and predictor models are derived for the March 4th data and T_W is set at 1s. The steady-state value of the rms power error was calculated for T_p = 1, 2 and 3s and for K_{ff} in the range 0 - 100. The results are shown in Fig. 13. This exhibits a trough at K_{ff} = 70 which is independent of T_p. For ideal feed-forward, a value of K_{ff} = 100 (for α = 0.01) would be expected from (28); the deviation of the optimum K_{ff} from this value is an indicator of the quality of the feed-forward signal. When K_{ff} = 70, the rms power error is seen to fall slowly as T_p increases. The minimum of 0.81MW rms occurs

when T_p = 3s, a 70% improvement on feedback alone. It is clear, however, that there is little to gain by trying to extend this particular predictor to look further ahead in time.

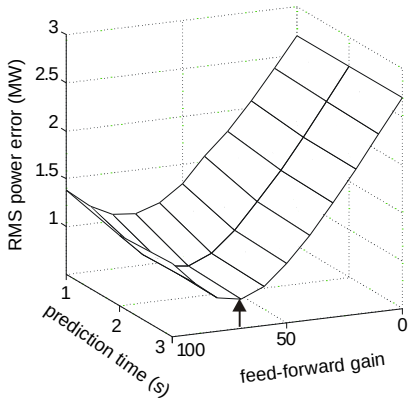

Fig. 13 RMS value of power error as a function of the prediction time and feed-forward gain; the arrow shows the minimum error over the range of values considered.

B. Effect of model mis-match

Feed-forward depends on the use of an approximate open-loop inverse and is susceptible to mis-match between the model and the actual plant. In this case, the water starting time T_W changes with operating point in the range 0.7 - 2.7s. The effect on the rms power error is shown in Fig. 14 where T_p = 2s throughout. First, note that the rms power error deteriorates as T_W increases even when there is only feedback present (K_{ff} = 0). This is to be expected because it becomes a more difficult system to control.

When T_W = 0.7s, the minimum error of 0.59MW occurs at K_{ff} = 80 which suggests that the feed-forward signal is very effective, allowing almost the full feed-forward to be used. When T_W = 2.7s, the minimum error of 2.68MW occurs at K_{ff} = 50 which suggests that the feed-forward signal is now less effective. Nevertheless, even for the worst-case T_W, it is seen to reduce the power error from 3.78MW with feedback alone to 2.68MW, an improvement of 29%.

Naturally, in practice, it will be necessary to base the predictor model on a day other than the current one - the previous day seems the most sensible selection, because the Grid characteristics vary slowly with season. To test sensitivity to discrepancies between the actual Grid and the predictor model, the prediction errors were computed for the same conditions as described in section IV.C but using a predictor based on an ARMAX969 model identified for September 1st instead of March 4th. The Grid model was fixed at its March 4th parameters. The results are shown in Table II and comparison with Table I shows that the frequency predictions do deteriorate although they remain better than the 'trivial' predictor.

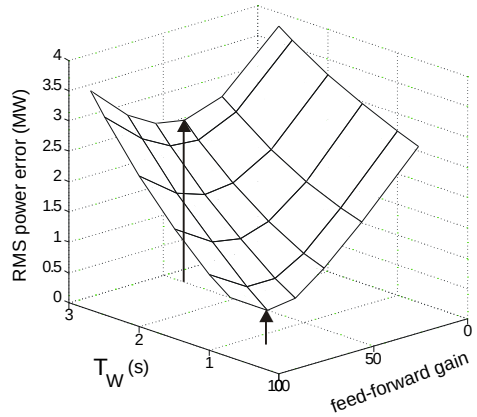

Fig. 14 RMS value of power error as a function of the water staring time and feed-forward gain. The minima for T_W = 2.7s (large arrow) and T_W = 0.7s (small arrow) are shown.

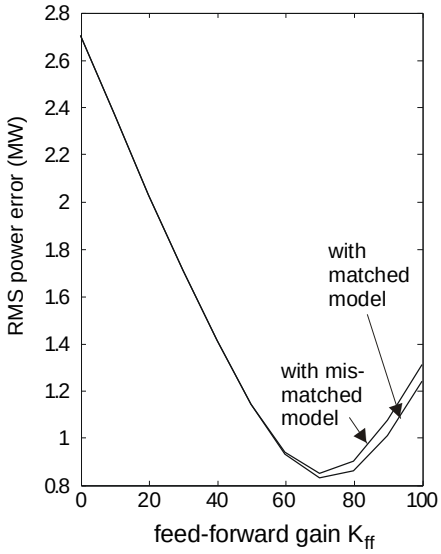

Fig. 15 Effect of mis-match between predictor model and actual system on the rms power error, as a function of feed-forward gain.

TABLE II

PREDICTION ERRORS WHEN USING THE INPUT RECORD FROM MARCH 4TH AND THE PREDICTOR MODEL FOR SEPTEMBER 1ST.

time ahead (s)	r.m.s. prediction error $\times 10^{-4}$	R^2 (%)	J^2 (%)
1/3	0.0053	99.9	94.8
1	0.114	98.9	42.9
2	0.309	97.2	-6.6
3	0.308	97.2	16.8

The September 1st predictor was then substituted into the simulation and the rms power error computed for T_p = 2s, T_W = 1s and K_{ff} in the range 0 - 100. Fig. 15 shows that, compared to the case when the nominal predictor is used, the loss in tracking error is not great, being most pronounced at large values of K_{ff}. This suggests that the feed-forward control scheme is not unduly sensitive, at least to small model errors.

VI. CONCLUSIONS

In this paper it has been shown that predictive feed-forward control can achieve a substantial improvement in tracking a power target when a hydroelectric station operates in PLR mode. The feed-forward controller is shown to be particularly effective in reducing power tracking error for values of water starting time (T_W) in the range 0.7 - 1.5s which correspond to 1 - 3 Units on-line. This covers more than 60% of Dinorwig's operation. Modest but worthwhile improvement is also obtained for higher values of T_W. A sensitivity analysis has shown that the controller is not unduly sensitive to using a predictor based on a model identified for another day.

An advantage of the feed-forward controller is that it is relatively easy to implement and commission. It does not require any changes to the well-tested feedback controller currently in use and can be switched in or out as necessary during operation. This makes testing easy and relatively safe, which is important when there are severe financial consequences if the plant should fail during operation. A possible drawback is that the controller produces more movement of the guide vane and could contribute to mechanical wear. A PC-based real-time version of the frequency predictor is currently being implemented and will be used over a period of several months to confirm the quality of the predicted values. In the meantime, a spare governor PLC will be re-programmed to include the feed-forward loop to test the integrity of the software. Finally, the scheme will be tested on a single live Unit.

ACKNOWLEDGMENT

The authors wish to thank Edison Mission Energy who funded this work by means of a research grant. Particular thanks are due to Dr Capell Aris and Mr Arwel Jones for their support and assistance.

REFERENCES

[1] P. Kundur, *Power system stability and control*, McGraw Hill, 1993.
[2] IEEE Working Group. "Hydraulic turbine control models for system dynamic studies", *IEEE Trans Power Systems* (1) 167-179, 1992.
[3] S.P. Mansoor, D.I. Jones, D.A. Bradley, F.C. Aris and G.R. Jones. "Reproducing oscillatory behaviour of a hydroelectric power station by computer simulation", *Control Engineering Practice*, **8**, 1261-1272, 2000.
[4] P.M. Anderson and M. Mirheydar. "A low-order frequency response model", *IEEE Trans Power Systems* **5**(3), 720-729, 1990.
[5] L. Ljung. System *identification – Theory for the user 2nd ed*, Prentice Hall, 1999.
[6] L. Ljung. *Systems Identification Toolbox v5 – User's Guide*, The MathWorks Inc, Natick MA, USA, 2000.
[7] G.F Franklin, J.D. Powell and M.L. Workman. *Digital Control of Dynamic Systems 2nd ed*, Addison-Wesley, 1990.
[8] MathWorks. Control *System Toolbox v5 – User's Guide*, The MathWorks Inc, Natick MA, USA, 2000.
[9] G.C. Goodwin, S.F. Graebe and M.E Salgado. *Control System Design*, Prentice Hall, 2001.